Research

Simulation test on shaft deformation induced by mining subsidence under similar gravity field in deep soil strata

Xu Han[1,2] · Zhe Qin[1,2] · Ji-huan Han[1,2] · Wei-hao Yang[3] · Yong-de Liu[1,2] · Jian Zhang[4]

Abstract

Many shafts in China have experienced large deformations in the deep soil Strata, which has had a significant impact on mining safety. This study conducted a geotechnical model test called the seepage force model to address the deformation issues of shafts caused by mining solid mineral resources in regions with deep soil strata. This test simulated the impact of mining disturbance on shaft deformation within the soil section. The simulation utilized monitoring data from the model shaft, facilitating the determination of deflection displacements across different protection areas. The findings indicated a nearly linear relationship between the maximum horizontal displacement of the shaft and the mining coal seam thickness. The shaft protection areas within the soil section were reconfigured by modifying the movement angle from 45° to 37.6°. Consequently, the maximum horizontal displacements of the prototype shaft decreased to 73.8, 112.7, and 170.9 mm for mining coal thicknesses of 2.7, 5.3, and 8.0 m, respectively. These values represent 26%, 24.6%, and 26.7% reductions from the original design shaft displacements. When combined with the probability integral method, the simulation test results concerning the shaft protection rock pillars were exhaustively examined. This analysis paves the way for a more logical and reliable design approach for shaft protection rock pillars in areas characterized by deep soil and thin rock strata. The study findings hold immense significance in effectively mitigating and managing mining-induced subsidence disasters and ensuring the optimal design of shaft protection zones.

Article Highlights

1. This paper established a seepage force test model, which realised the simulation of gravity field in a 600 m deep soil strata, to carry out experimental research on the shaft deformation induced by mining subsidence, and the simulated soil thickness is the largest.
2. The test adopts strain gauge and distributed optical fibre sensing test method to measure the strain data at different depths of the shaft, with advanced monitoring means and high accuracy of measurement data.

✉ Ji-huan Han, hanjh@sdust.edu.cn; Xu Han, hx1143909328@163.com; Zhe Qin, chin@sdust.edu.cn; Wei-hao Yang, whyang@cumt.edu.cn; Yong-de Liu, 1667281063@qq.com; Jian Zhang, kjzhangjian@126.com | [1]Shandong Key Laboratory of Civil Engineering Disaster Prevention and Mitigation, Shandong University of Science and Technology, Qingdao 266590, China. [2]College of Civil Engineering and Architecture, Shandong University of Science and Technology, No.579 Qianwangang Road, Huangdao District, Qingdao 266590, Shandong, China. [3]State Key Laboratory for Geomechanics and Deep Underground Engineering, China University of Mining and Technology, Xuzhou 221116, China. [4]Shandong Energy Group Luxi Mining Co. LTD, Heze Shandong 274000, China.

3. The findings of this research contribute to a more scientific and reliable design method for the shaft protection areas in the deep soil strata, which addresses the limitations of using measured movement angles in the design of shaft protection rock pillars.

1 Introduction

China possesses abundant solid mineral resources, including coal and iron, with reserves surpassing hundreds of billions of tons [1]. In order to exploit these deep-seated mineral resources, 88 deep vertical shafts have been constructed, with soil thicknesses exceeding 400 m; the maximum soil thickness recorded is 754.98 m. Of these shafts, 89% penetrate soil layers thicker than rock layers. The shaft, often termed the "throat" of the mining operation, is integral to the safety of the entire coal mine [2–5]. As mining depth has increased in recent years, shaft deformation in deep soil strata has become more pronounced [6–13]. For instance, as of August 2017, the primary and auxiliary shafts in the Guotun Coal Mine displayed significant deviations of 359 mm and 322 mm, respectively. Such pronounced shaft deflection in the soil layer is unparalleled in China and rare in global mining history. Similarly, the auxiliary shaft's maximum deviation reached 78 mm in the Zhao Coal Mine in December 2018. Such deformations not only disrupt regular hoisting operations but also compromise the safety of the shaft lining.

To ensure mining activities do not affect the shaft's safety and utility, a protective rock (including coal) pillar must be established per specifications. Most of China's shaft protection zones in soil sections are designed based on a 45° movement angle. However, current guidelines for determining shaft protection zones stem from extensive observations of surface movement dynamics in thin soil and thick rock strata, limiting their relevance to newly established shafts in deeper soil strata. This often results in an inadequately protected area, rendering the shaft susceptible to mining activity-induced damage [14, 15].

Similar material model tests have been widely employed to accurately depict stratigraphic movement during solid mineral mining. These tests study the movement of overburden rock in the void left by mining. Zuo et al. [16] simulated a rock stratum thickness of 164.02 m to analyze the effects of deep mining on fault activation and the evolution of induced fault zones in the Huainan Mine. Hu et al. [17] simulated a stratum l450 m thick (with only 10 m of soil) to assess the subsidence of overlying rocks in the Tashan Coal Mine. Liu et al. [18] employed a mixture of sand and sawdust to simulate loose strata with comparable bulk density, revealing the movement mechanisms of 400 m deep loose and rock strata two-layer medium under mining influence. However, most research has centered on the subsidence patterns of overlying rocks, with limited studies on the movement dynamics of rock in deep soil strata. In addition, using the equivalent load method in model tests to account for gravity does not ensure congruity in internal gravitational fields, introducing potential distortions in test outcomes. Hence, it is imperative to perform physical model tests under analogous gravitational conditions to capture mining's impact on shaft deformation.

As a special underground structure traversing intricate geological formations, the shaft resembles a distinct "pile" structure embedded in rock strata. Therefore, the seepage force of water simulates the gravity field of these layers, drawing upon the soil mechanics seepage force tests employed in pile foundation stability analysis. This method was introduced by A. Zelikson et al. [19] in France in the early 1960s. Ding et al. [20] pioneered applying this approach to pile foundations and shallow buried structures in China. Since then, it has become prevalent in the stability analysis of pile foundations [21, 22]. Although hydraulic permeation soil mechanics tests can simulate the gravity field of the soil strata, their utilization in simulating the gravity stress field of deep soil strata remains limited. This study uses shaft deflection in the Guotun Coal Mine in Shandong Province as a model, suggesting the adoption of hydraulic permeation to simulate the gravity stress field of deep soil strata, and conducted high-pressure hydraulic percolation force model tests. Combined with the deformation law of the rock strata, a sector-shaped hydraulic pillow is developed to simulate the deformation of rock masses resulting from mining. The study realised the simulation of shaft deformation induced by mining subsidence under similar conditions of gravity field in deep soil strata, and shed light on the deformation patterns of shafts in the soil strata segment when affected by mining operations.

2 Design of similarity model

2.1 Derivation of similarity criterion

Considering the various factors that influence the shaft's deformation pattern during coal seam excavation, the parameter equation is determined as follows:

$$F(l_r, s_r, h_s, h_c, m_r, B, d, D_w; \rho_w, \rho_{sf}, \rho_s; g; E_s, E_c; \varepsilon, \mu, i_w), \tag{1}$$

where l_r, s_r, and m_r are the length in the strike direction, length in the dip direction, and maximum subsidence height of the overlying strata in the goaf, respectively; h_s is the thickness of the soil strata; h_c is the depth of the shaft; B is the dimensions of the shaft protection rock pillars; D_w and d are the inner and outer diameters of the shaft, respectively; ρ_w and ρ_s are the densities of water and soil, respectively; ρ_{sf} is the buoyant density of the soil; g is the acceleration due to gravity; E_s and E_c are the elastic moduli of the soil and shaft lining, respectively; ε is the strain of the shaft lining; μ is the Poisson's ratio of the soil; i_w is the hydraulic gradient.

Based on Eq. (1), the derived similarity criteria [23] are as follows:

Dimensionless criteria: $\Pi_1 = \varepsilon$, $\Pi_2 = \mu$, $\Pi_3 = i_w$.

Geometric criteria: $\Pi_4 = l_r/h_s$, $\Pi_5 = s_r/h_s$, $\Pi_6 = h_c/h_s$, $\Pi_7 = m_r/h_s$, $\Pi_8 = B/h_s$, $\Pi_9 = d/h_s$, $\Pi_{10} = D_w/h_s$.

Mechanical criteria: $\Pi_{11} = E_c/E_s$.

Other criteria: $\Pi_{12} = \rho_{sf}/\rho_w$, $\Pi_{13} = \rho_s/\rho_w$.

The remaining parameters are h_s, ρ_w, E_s, and g. Since h_s, ρ_w, and g are dimensionally independent fundamental quantities, and E_s is a derived quantity, dimensional analysis can be applied to determine $\Pi_{14} = \rho_w g h_s/E_s$.

2.2 Prototype parameters

To design model tests more effectively and to define the research object and objectives, the deep soil strata of the Guotun Coal Mine were selected as the prototype strata. The parameter ranges that reflect the prototype strata in the model tests are determined as follows:

(1) The prototype strata comprise a single horizontal layer with a soil thickness of hs = 600 m.

(2) Referring to the main shaft of the Guotun Coal Mine, the concrete strength grade for the shaft lining varies between C30 and C75, with a mean strength grade of C50. The inner diameter of the shaft measures $d = 5$ m, while the outer diameter of the shaft's outer layer is $D_w = 9.5$ m. The depth of the shaft is $h_c \geq 600$ m.

(3) The coal seam is a single horizontal seam with a mining thickness ranging from $m = 3$ to 18 m, indicating that the maximum subsidence height of the overlying strata in the goaf is $m_r \leq 18$ m.

(4) The strike length, l_r, is at least 600 m, and the dip length, s_r, is at least 240 m for the surface subsidence of the overlying rock strata in the goaf.

(5) The size of the shaft protection rock pillars in the soil strata segment has been determined to be $B \geq 600$ m.

3 Establishment of the model test

3.1 Model test platform

The test was carried out utilizing the "Deep Underground Engineering Simulation Test Platform" at the State Key Laboratory for Geomechanics and Deep Underground Engineering, China University of Mining and Technology. The test platform has a net effective test size of $\phi 1200 \times 900$ mm and is assembled using the configuration depicted in Fig. 1, consisting of an upper sealing cover, upper taper ring, upper-end cover, pressure cylinder, lower-end cover, lower taper ring, and lower sealing cover. The arrangement of the monitoring elements and hydraulic pillows is shown in Fig. 2. Based on the prototype parameters, the shaft in the soil section is protected over a distance exceeding 600 m. The distance between the rock mass deformation zone and the cylinder wall should not be too small to avoid boundary effects during the test and considering

Fig. 1 Test platform assembly
effect drawing

(a) Vertical profile along I-I

(b) Horizontal profile along II-II

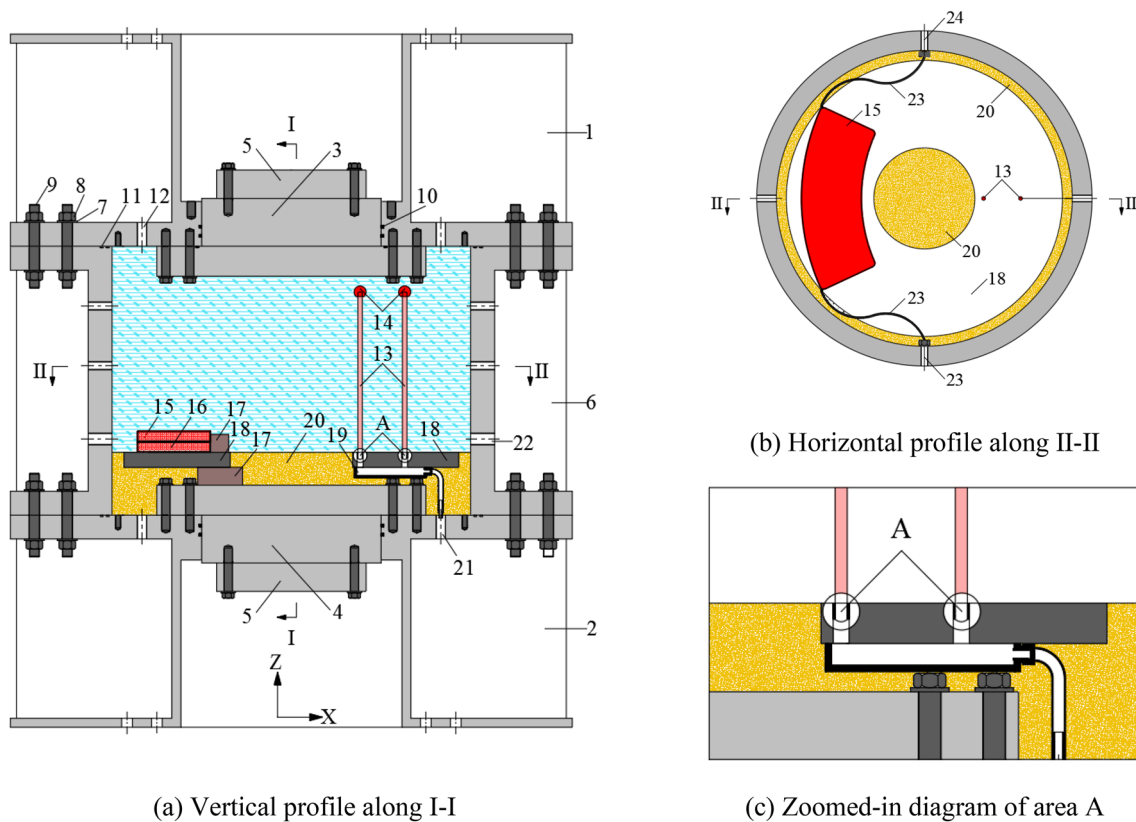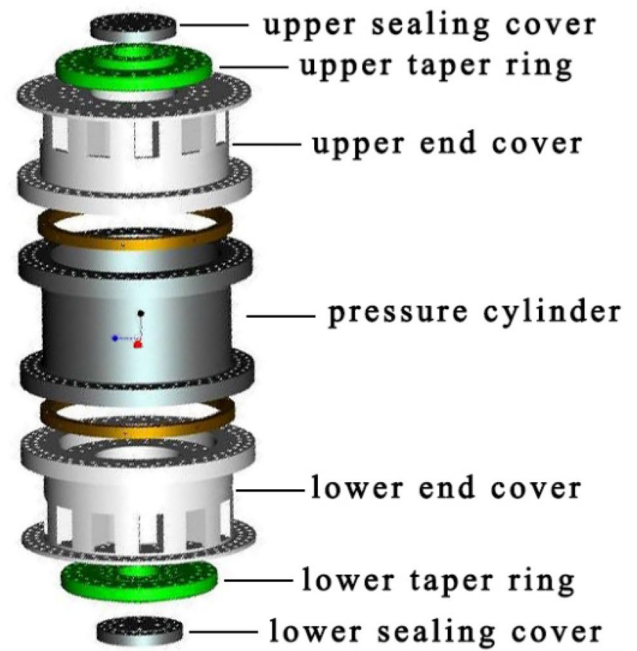(c) Zoomed-in diagram of area A

Fig. 2 The schematic diagram of the physical simulation test platform: 1—upper sealing cover; 2—lower sealing cover; 3—upper taper ring; 4—lower taper ring; 5—sealing plate; 6—pressure cylinder with reinforcing ribs; 7—flat washer; 8—hexagonal nut; 9—screw; 10—O-ring seal (600×7.0 mm); 11—O-ring seal (1220×7.0 mm); 12—inlet hole; 13—model shaft; 14—epoxy resin ball; 15—upper hydraulic pillow; 16—lower hydraulic pillow; 17—spacer block; 18—circular pressure steel plate; 19—fiber optic protection box; 20—clay filling layer; 21—outlet hole; 22—drain hole; 23—stainless steel high-pressure tubing; 24—oil outlet hole

that the deformation zone of the rock mass during mining is larger than the size of the goaf. The geometric similarity ratio C_L was determined by combining the above analyses with the effective space of the test platform as 1200. Moreover, the corresponding geometric dimensions of the model test are shown in Table 1.

3.2 Model strata

Clay and fine sand were chosen as the model strata with a specific mass ratio, considered the prototype material. Then, it is consistently observed that the dimensionless criterion Π_2 remains satisfied [23]. In addition, inferences from $\Pi_{11}\Pi_{14}$ suggest that

$$C_{E_s} = 1, C_{\rho_s} = 1, C_{\rho_{sf}} = 1, C_{\rho_w} = 1, C_{\rho_w}C_g C_{h_s}/C_{E_s} = 1, \tag{2}$$

where $C_{E_s}, C_{\rho_s}, C_{\rho_{sf}}, C_{\rho_w}, C_{h_s}$, and C_g are the ratios of elastic modulus, density, buoyant density, water density, soil thickness, and gravity acceleration between the prototype and model strata, respectively.

Based on the geometric similarity ratio $C_L = C_{h_s} = 1200$, then

$$C_g = \frac{1}{C_{h_s}} = \frac{1}{1200}. \tag{3}$$

If the vertical effective stress at depth z_1 in the model stratum equals the gravity stress at depth z_2 in the prototype strata, then

$$\left(f_s + \rho_{sf}g\right)z_1 = \rho_{sf}gz_2, \tag{4}$$

$$f_s = \rho_w g i_w, \tag{5}$$

where f_s is the seepage force; i_w is the hydraulic gradient; ρ_w is the water density; g is the gravitational acceleration; ρ_{sf} is the soil buoyant density.

By combining Eqs. (4) and (5), the following can be derived:

$$i_w = \left(\frac{z_2}{z_1} - 1\right)\frac{\rho_{sf}}{\rho_w} = \left(C_{h_s} - 1\right)\frac{\rho_{sf}}{\rho_w} = 1199\frac{\rho_{sf}}{\rho_w}. \tag{6}$$

Given that soil density is roughly double that of water, or $\rho_{sf}/\rho_w \approx 1$, it can be inferred that $i_w = 1199$ from Eq. (6). The hydraulic pressure difference between the model stratum's top and bottom surfaces can be set at 6 MPa. For the model test to meet the criteria of both a high hydraulic gradient and a consistent hydraulic gradient, the mass ratio of clay (Fig. 3) to fine sand (Fig. 4) should be 1:1. This ratio can simulate a stable percolation pressure of 6 MPa in a 0.5 m thick layer with a controllable percolation volume.

3.3 Model shaft

Polyoxymethylene (POM) rods were selected as the simulated casing material for the shaft. The elasticity modulus of this material was measured at $E_{c0} = 2.6$ GPa. By utilizing solid rod elements with equivalent flexural stiffness in place of the cylindrical structure of the casing, both the prototype and model shaft met the specified criteria.

$$E_p I_{z0} = E_c I_z \tag{7}$$

Table 1 Geometric dimensions of model test	Name	C_L	h_s (m)	m (m)	l_r (m)	s_r (m)	h_c (m)	B (m)
	Prototype	1200	600	3–18	≥ 600	≥ 240	≥ 600	≥ 600
	Model	1	0.5	0.0025–0.015	≥ 0.5	≥ 0.2	≥ 0.5	≥ 0.5

Fig. 3 Clay particles

Grain size=0.01~0.05 mm

Fig. 4 Fine sand particles

Grain size=0.074~0.4 mm

$$I_z = \frac{\pi\left(D_w^4 - d^4\right)}{64}, I_{z0} = \frac{\pi D_{w0}^4}{64} \tag{8}$$

where I_{z0} is the moment of inertia of the solid shaft material; D_{w0} is the equivalent outer diameter of the solid shaft material.

Based on the prototype parameters $E_c = 34.5$ GPa, $d = 5$ m, and $D_w = 9.5$ m, the equivalent outer diameter $D_{w0} = 17.8$ m can be determined by solving Eqs. (7) and (8). The result was approximately 14.8 mm using the similarity ratio to calculate the model shaft diameter. Therefore, a POM rod with a diameter of $\phi15$ mm was selected as the material for the model shaft.

3.4 Calibration of hydraulic pillow

The test simulates the subsidence process of the underlying rock mass using hydraulic pillows to regulate oil pressure. Constructed by welding Q235 steel plates with a thickness of 3 mm, these hydraulic pillows have a fan-shaped design with an axial effective length of 240 mm and an effective height of 30 mm for the internal cavity. The study employs a double-layer hydraulic pillow design for enhanced settlement results, releasing pressure sequentially from top to bottom. Before the test, researchers conduct quantitative performance tests to ensure that the hydraulic pillows demonstrate reliable sealing and deformation characteristics. Displacement sensors calibrate the deformation of the hydraulic pillows. Figure 5 presents the calibration of the hydraulic pillows, whereas Fig. 6 depicts the relationship curve between deformation displacement and oil volume.
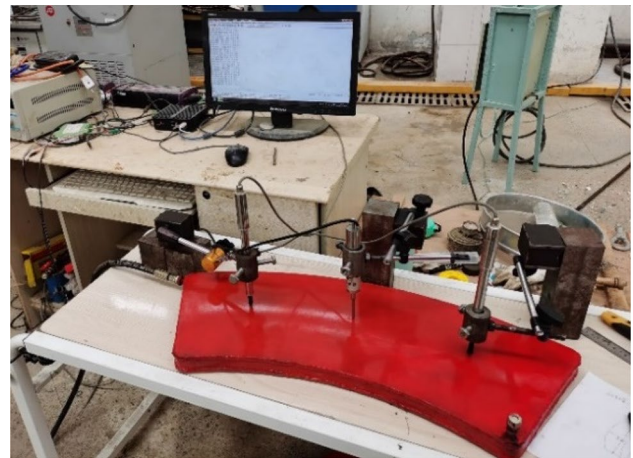
Fig. 5 Hydraulic pillow

Fig. 6 Relationship curves between deformation displacement and oil return volume of the hydraulic pillow
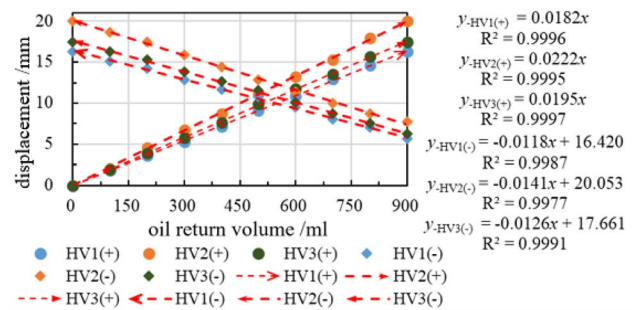

Fig. 7 Vertical layout of strain gauges and optical fiber

3.5 Data acquisition system

Direct measurement of the displacement process of the model shaft was infeasible due to the closure of the test rig. Therefore, this study adopted two monitoring methods to infer displacement changes by monitoring strain variations in the shaft. The methods used were resistance strain gauges and distributed optical fiber. The resistance strain gauges chosen were of model BA120-05AA-A150(16)-Q30, with a sensitive grating size of 0.5×1.2 mm. Two model shafts, denoted as 1# shaft and 2# shaft, were employed on the test platform. Each shaft had five layers of strain gauges, with four measuring points per layer. Data collection was conducted using a static strain testing instrument. The distributed optical fiber had a diameter of 0.8 mm, was armored, and allowed for adjustable spacing

Fig. 8 Profile layout of strain gauges and optical fiber
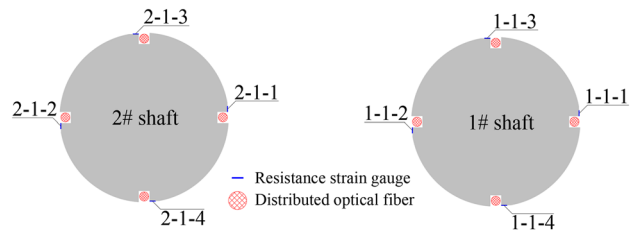
Fig. 9 Position calibration of an optical fiber test segment
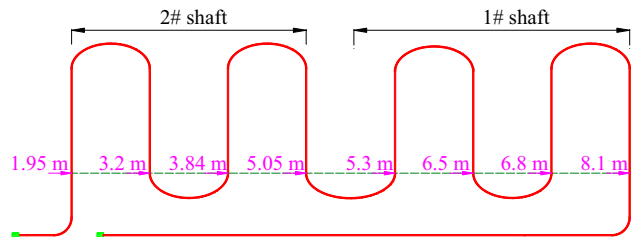
between measuring points based on test requirements. Data was collected using an ODiSI-A acquisition instrument. The arrangement of the strain gauges and the optical fiber is depicted in Figs. 7 and 8. The calibration results for the optical fiber test segment are shown in Fig. 9. Notably, the identifier '2–1–3' represents the third strain gauge in the first layer of the #2 model shaft. This notation convention is consistent for other strain gauges, and the suffix "f" indicates the corresponding fiber measurement point at the same position as the strain gauge.

Using the bottom end of the effective test segment of the model shaft as the origin of the vertical axis z, and progressing the direction towards the surface, strains at the symmetric locations of the model shaft inclined in the direction of deviation are $\varepsilon_a(z)$ and $\varepsilon_b(z)$, respectively. The general solution to the flexural equation of the model shaft is provided by analyzing the deviation of the model shaft due to mining as a pure bending problem.

$$u(z) = \int_0^z \int_0^z \frac{\varepsilon_a(z) - \varepsilon_b(z)}{d_m} dz dz + C_1 z + C_0, \tag{9}$$

where $u(z)$ is the horizontal displacement of the model shaft at the z-coordinate point, $\varepsilon_a(z)$ and $\varepsilon_b(z)$ are the tensile strain and compressive strain of the model shaft at the z-coordinate point, respectively, d_m is the diameter of the model shaft, C_0 and C_1 are both integration constants.

When the model shaft is considered an equivalent cantilever beam structure with horizontal constraints at the bottom, it can be deduced from the boundary conditions that $C_0 = C_1 = 0$. For the distributed optical fiber, its test intervals are extremely small. As a result, the horizontal displacement of the shaft can be indirectly estimated from its strain results.

$$u(z) = \sum_{j=0}^{z/\Delta z_j} \left\{ \sum_{i=0}^{j} \left[\frac{\varepsilon_a(z_i) - \varepsilon_b(z_i)}{d_m} \Delta z_i \right] \right\} \Delta z_j, \tag{10}$$

where Δz_i and Δz_j are the test intervals of the distributed optical fiber.

4 Process of model test

The test process comprises four primary stages: test layout, consolidation with pressurized drainage, saturation of the vacuum soil layer, and simulation of mining subsidence.

4.1 Test layout

(1) Strain gauge and fiber optic installation

Strain gauges are attached to the designated positions using cyanoacrylate adhesive, and the surface of the gauges and wire connections are coated with sealing adhesive HH-703 to prevent short-circuiting, as depicted in

Fig. 10 Strain gauge buried


Fig. 11 Sealing glue on model shaft

Fig. 10. The model shaft is secured to the pressure plate, and the optical fibers are affixed within the groove using cyanoacrylate adhesive in a spot-fastening method. To ensure protection, an even layer of AB glue is applied to the model shaft's surface, providing a protective layer for both the strain gauges and optical fibers, as illustrated in Fig. 11. In addition, the fiber optic protection box is installed beneath the pressure plate, as depicted in Fig. 12.

(2)   Model shaft and hydraulic pillow installation

Fig. 12 Optical fiber protection

Fig. 13 Location arrangement of the model shaft and hydraulic pillow

(a) Unfilled soil   **(b)** Filled soil following tamping
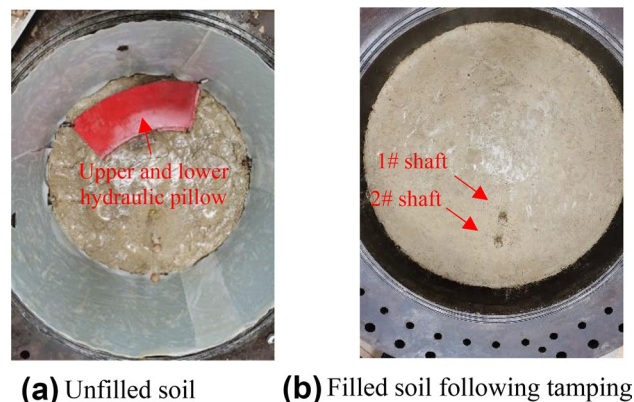
Model shafts are designated based on their proximity to the centerline of the test platform, with the 1# shaft being closer to the centerline and the 2# shaft situated further away. Both shafts are embedded in a ring-shaped pressure plate with a thickness of 50 mm. The initial embedment depth of the shafts into the pressure plate is 25 mm. Hydraulic pillows are stacked and placed on the surface of the pressure plate. The distances from the hydraulic pillows to the #1 and #2 shafts are 500 and 650 mm, respectively. The total length of the model shafts is 575 mm, and the gap between the two shafts is 150 mm. The arrangement of the model shafts and hydraulic pillows in this test is displayed in Fig. 13a. After positioning the hydraulic pillows and model shafts, the soil is compacted layer by layer, and the consolidation settlement is determined to ensure that the final soil thickness aligns with the design requirements, as indicated in Fig. 13b.

Fig. 14 Unloading process of a hydraulic pillow by oil return

Fig. 15 Oil return volume of a hydraulic pillow with time
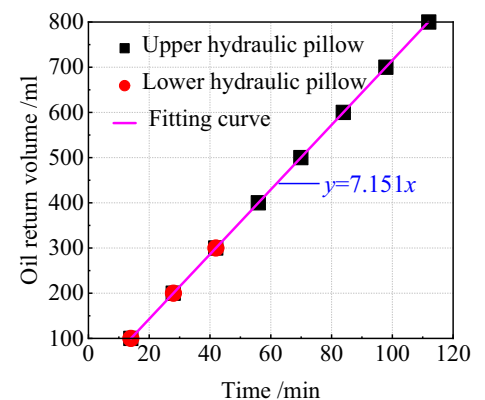
4.2 Simulation of mining subsidence

After completion of the pressurized drainage consolidation and vacuum saturated soil layer, a servo-compression and stabilization system was utilized to apply the seepage pressure. When the seepage pressure reached 5.7 MPa, water droplets emerged at the outlet. Simultaneously, the pressure gauge on the drainage pipe consistently registered a reading of 0 throughout the seepage phase. Test results indicated that stable seepage can be maintained within a 5.8 to 6.5 MPa pressure range. After holding the seepage pressure at 6 MPa for 10 min, the oil return process for the hydraulic pillow commenced by manually operating the hand pump, as depicted in Fig. 14. Each hand pump cycle released 100 ml of oil, adhering to the principle of first releasing the upper hydraulic pillow followed by the lower one. The total cumulative oil release for the upper and lower hydraulic pillows was 800 and 300 ml, respectively. The relationship between the cumulative oil release from the hydraulic pillows and the cumulative oil release time is illustrated in Fig. 15. The average manual oil release rate was determined to be 7.151 ml/min. A 15-min stabilization period followed each oil release cycle to ensure adequate subsidence induced by mining.

Fig. 16 Surface subsidence measurement
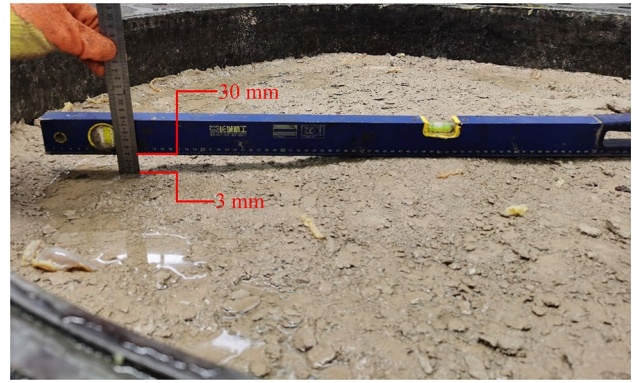
5 Analysis of test results

5.1 Simulation effect of the hydraulic pillow

Based on the calibration results for the hydraulic pillow, it was determined that when the total volume of oil returned reached 1100 ml, the combined settlement displacement at the HV2 measuring points of the upper and lower hydraulic pillows was 24.4 mm. Concurrently, Fig. 16 shows that the measured surface subsidence is 27 mm. Considering the influence of consolidation settlement during the seepage stage, the measured value aligns closely with the calibrated value. This indicates that the hydraulic pillow models can effectively simulate the effects of mining-induced subsidence in the geological strata.

5.2 Validation of test results

The distributed fiber-optic monitoring data calculated the strain differences between measurement points 1f and 2f, and 3f and 4f of the model 1# and 2# shafts at the same horizontal level and mining stages for the model shafts. The results are presented in Figs. 17 and 18, respectively. The horizontal displacement curves for the model shafts, calculated using Eq. (11), are shown in Figs. 19 and 20, respectively. Analyzing the total horizontal displacement of the model shafts can infer the prototype shaft's horizontal displacement. The inversion results are displayed in Fig. 21. Additionally, in light of the calibration results for the hydraulic pillow, the settlement displacements of the corresponding measurement points on the surface of the prototype rock strata were calculated for different oil return volumes and are depicted in Fig. 22.
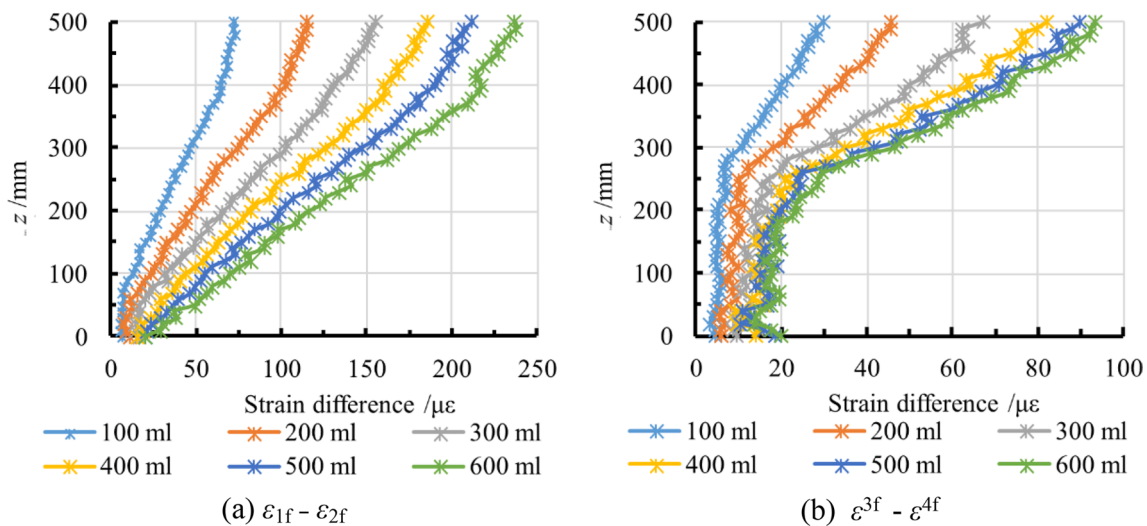

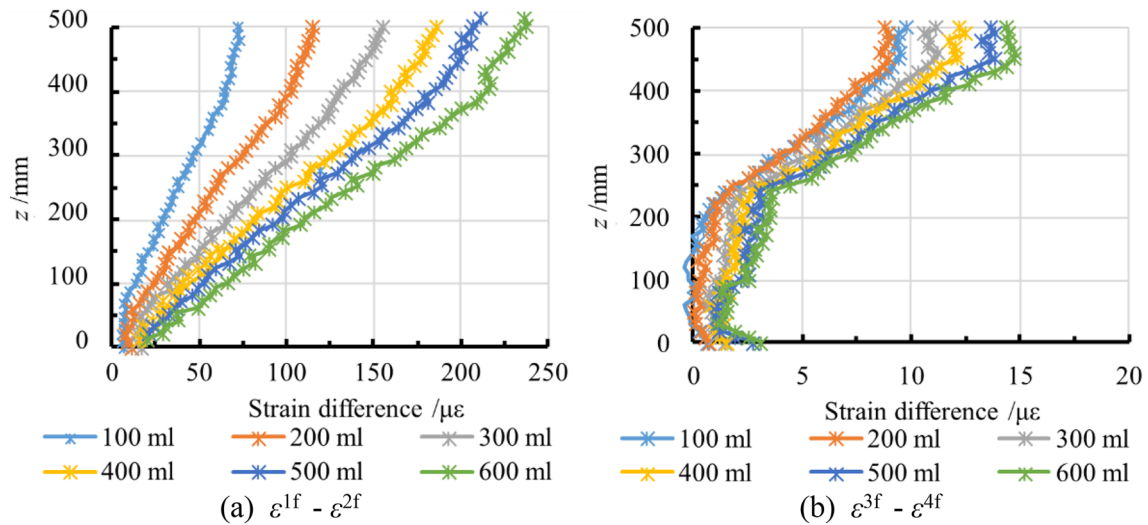**Fig. 17** The fiber strain difference of 1# model shaft at different stages

(a) $\varepsilon_{1f} - \varepsilon_{2f}$ (b) $\varepsilon^{3f} - \varepsilon^{4f}$

Fig. 18 The fiber strain difference of 2# model shaft at different stages
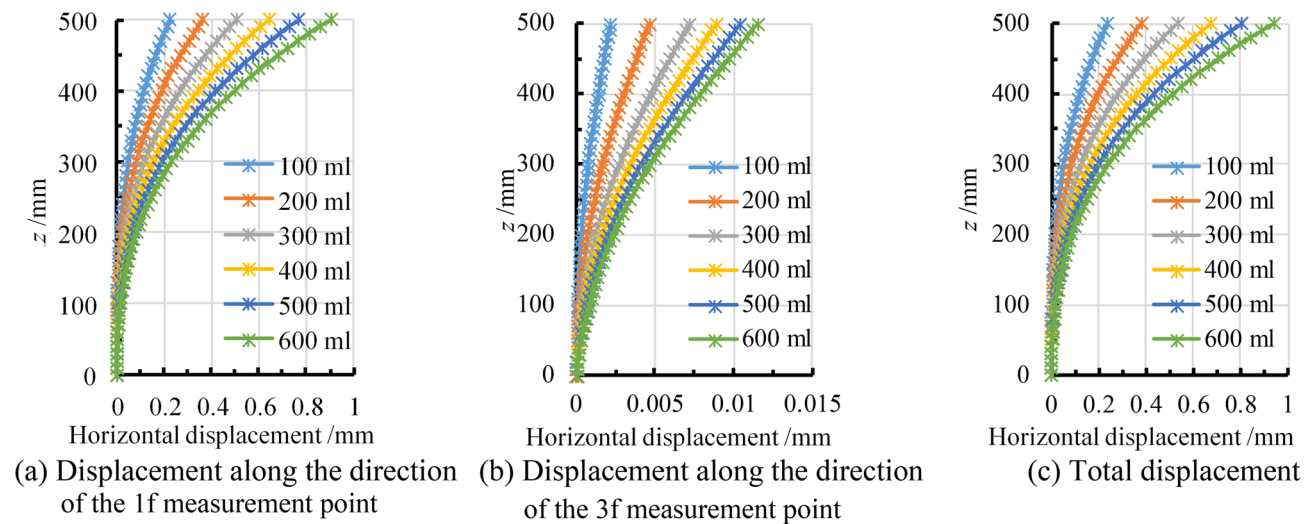

Fig. 19 Horizontal displacement of 1# model shaft during different mining stages

Based on the movement patterns of the curved zone in deep soil and thin rock strata, the maximum settlement displacement (at the HV2 measurement point) of the hydraulic pillow mirrors the maximum deflection of the rock strata in the curved zone. This deflection value is roughly equivalent to the thickness of the coal seam during mining. Thus, using the maximum settlement displacement of the hydraulic pillow to estimate the mining thickness of the prototype coal seam is reasonable.

5.3 Exploration of test results

Based on the comprehensive analysis of Figs. 21 and 22, the following conclusions can be derived:

(1) The maximum horizontal displacement of the model shaft increases approximately linearly with the increase in the oil return volume of the hydraulic pillow. When the oil return is 100 ml, the maximum horizontal displacements of shafts #1 and #2 are 238.8 mm and 73.8 mm, respectively. With an oil return of 600 ml, the maximum horizontal displacements of shafts #1 and #2 are 1127.5 mm and 280 mm, respectively. The slopes are approximately equal to 1.703 and 0.439, respectively. This finding indicates a roughly linear proportional relationship between the maximum
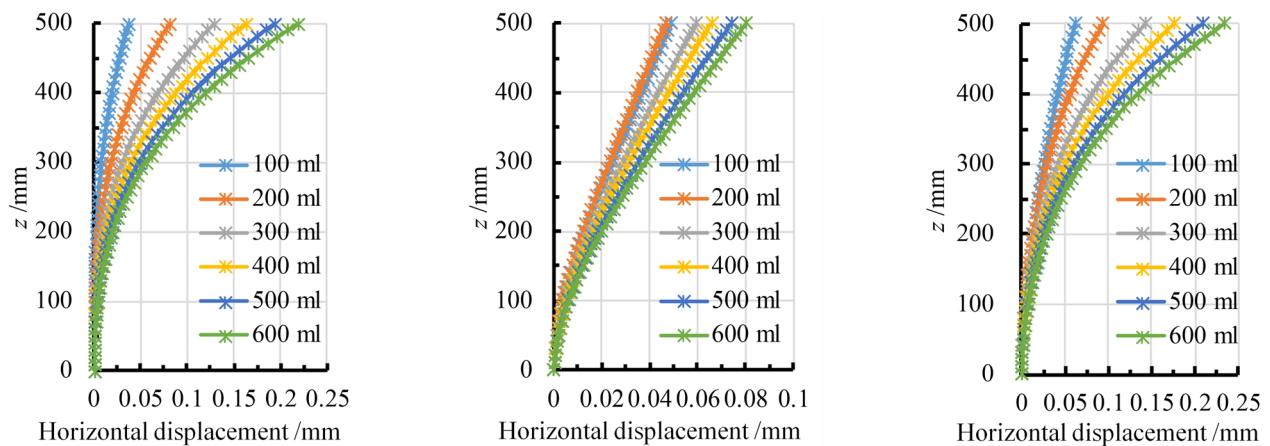
(a) Displacement along the direction of the 1f measurement point

(b) Displacement along the direction of the 3f measurement point

(c) Total displacement

Fig. 20 Horizontal displacement of 2# model shaft during different mining stages

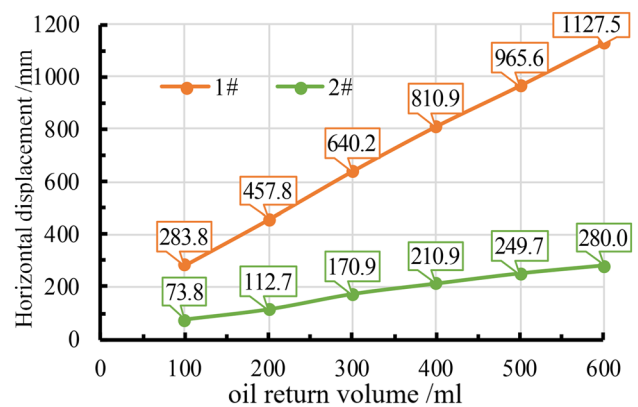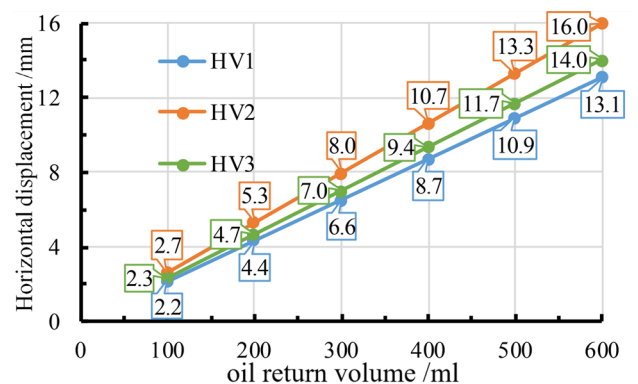**Fig. 21** Maximum horizontal displacement of prototype shaft with different oil return volume

Fig. 22 Subsidence displacement of prototype rock surface with different oil return volume

horizontal displacement of the shaft and the coal seam's thickness. Such a relationship aligns with the deflection pattern of the shaft observed during mining under conditions of thick soil and thin rock formations.

(2) In designing the protection area for a soil strata section shaft with a displacement angle of 45°, one can draw analogies from the situation of the #1 model shaft during the test. With an oil return volume of the hydraulic pillow at 100 m³, simulating an excavation thickness for the prototype coal seam at 2.7 m, the calculated maximum horizontal displacement for the prototype shaft is 283.8 mm. Considering that the shaft displacement is proportional to the excavation thickness of the coal seam when the mining thickness of the prototype coal seam is simulated at 3.5 m,

the inverted maximum horizontal displacement of the prototype shaft can reach 367.9 mm, while the maximum deflection of the primary shaft of the Guotun coal mine is 359 mm. This outcome aligns closely with data from the Guotun Coal Mine, indicating that the test results in this chapter are reliable and have significant engineering application value.

(3) For designs with a displacement angle of 37.6° in the protection area of the soil strata section shaft, parallels can be drawn from the situation of the #2 model shaft during testing. When simulating excavation thicknesses for the prototype coal seam at 2.7, 5.3, and 8.0 m, the calculated maximum horizontal displacements for the prototype shaft are 73.8, 112.7, and 170.9 mm, respectively. These displacements represent 26%, 24.6%, and 26.7% of the displacement observed in the #1 model shaft. Consequently, by suitably adjusting the value of the displacement angle in the shaft protection rock pillar design, one can effectively reduce the shaft deflection displacement.

The probability integration method offers a suitable approximation to estimate the surface displacement at locations outside of the shaft's position. Designating the surface point directly above the goaf boundary as the x-axis origin, with the positive x-direction oriented towards one side of the shaft, the formula to predict surface movement at a given x-coordinate can be determined using the probability integration method [24] as follows:

$$u(x) = u_0 e^{-\pi \frac{x^2}{r^2}}, \tag{11}$$

$$u_0 = b w_0, \tag{12}$$

where u_0 is the maximum horizontal displacement at the surface point.

When ignoring the rock strata, the edge of the hydraulic pillow in the model test can serve as the boundary of the coal mining. If x_0 represents the abscissa of any point on the surface, and x_{01} and x_{02} denote the abscissas of the surface points for the model shafts #1 and #2 in the prototype stratum, Eq. (11) can be employed to derive the following expression:

$$u_0 = u(x_{01}) \left[\frac{u(x_{01})}{u(x_{02})} \right]^{\frac{x_{01}^2}{x_{02}^2 - x_{01}^2}}, \tag{13}$$

$$r_0 = \sqrt{\pi(x_{01}^2 - x_{02}^2) \Big/ \ln\left[\frac{u(x_{02})}{u(x_{01})}\right]}, \tag{14}$$

$$x_0 = \sqrt{x_{01}^2 + (x_{01}^2 - x_{02}^2)\ln\left[\frac{u(x_0)}{u(x_{01})}\right] \Big/ \ln\left[\frac{u(x_{01})}{u(x_{02})}\right]}. \tag{15}$$

Figure 21 depicts the values of $u(x_{01})$ and $u(x_{02})$ for different excavation states when $x_{01} = 600$ m and $x_{02} = 780$ m. Equations (13) and (14) yield the inverse values of u_0 and r_0 for various oil return volumes, illustrated in Figs. 23 and 24, respectively.

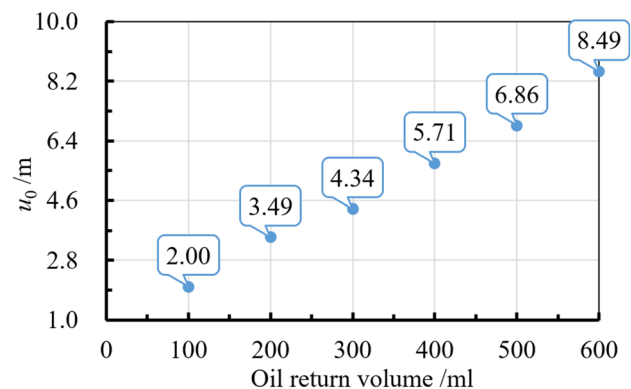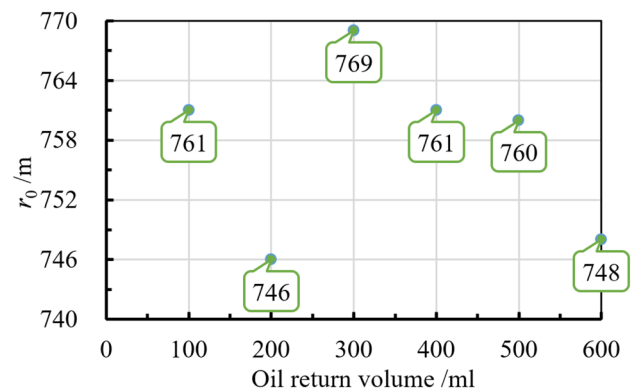**Fig. 23** Inverse values of u_0 with different oil return volumes

Fig. 24 Inverse values of r_0 with different oil return volumes

Using the data for the maximum horizontal displacement of the shaft in Fig. 21, Eq. (15) can be employed to calculate the abscissa of different surface points corresponding to distinct horizontal displacements. If $u(x_0)$ equals the critical deflection of the shaft under full excavation conditions, the value of x_0 can approximate the dimension of the shaft protection rock pillar in the soil section of the shaft.

6 Conclusion

(1) In preparing the model strata, the mass ratio of clay to fine sand is 1:1. This ratio allows the percolation hydraulic model to simulate the initial gravity stress field effectively with a soil thickness of 600 m. The hydrostatic pressure remains stable at a level exceeding 6 MPa throughout the percolation stabilization and simulated mining stages.

(2) The total settlement displacement at the center point of the two-layer hydraulic pillow is 24.4 mm, whereas the measured settlement displacement on the model strata surface is 27 mm. Given the consolidation settlement during the seepage stage, simulating mining disturbance using the hydraulic pillow's settlement is feasible, and the simulation results are satisfactory.

(3) A positive linear correlation exists between the shaft's horizontal displacement and the coal seam's thickness from mining. For the #1 and #2 model shafts, which correspond to the prototype shaft, the dimensions of the shaft protection rock pillars were 600 m and 780 m, respectively. When mining a coal seam with a thickness between 2.2 and 2.7 m, the maximum horizontal displacements of the shaft in the soil section were 284 mm for the #1 model shaft and 74 mm for the #2 model shaft. Similarly, for coal seam thicknesses of 4.4–5.3 m, the displacements were 458 and 113 mm, and for 6.6–8.0 m thicknesses, they were 640 and 171 mm, respectively. For coal seam thicknesses between 8.7 and 10.7 m, the displacements remained at 640 and 171 mm. Thus, it is evident that the design of the shaft protection rock pillars must account for the coal seam's thickness.

(4) Mining disturbances induce varying horizontal movements in the shaft at different depths. The shaft's displacement diminishes with depth, accounting for the primary reason behind shaft deflection. In addition, designing the shaft protection areas based on a movement angle of 45° in deep soil strata is unsuitable. Adjusting the movement angle based on actual coal mining conditions is advisable.

Data availability All data included in this study are available upon request by contact with the corresponding author.

Declarations

Ethics approval and consent to participate This study does not contain any studies with human participants performed by any of the authors.

Consent for publication All the authors have approved the manuscript for submission and publication.

Competing interests I would like to declare that the authors have no conflict of interests as defined by Springer, or other interests that might be perceived to influence the results and/or discussion reported in this paper.

References

1. Wu Q, Tu K, Zeng YF, Liu SQ. Discussion on the main problems and countermeasures for building an upgrade version of main energy (coal) industry in China. J China Coal Soc. 2019;44(6):1625–36. https://doi.org/10.13225/j.cnki.jccs.2019.0387.
2. Publicity and Education Centre of the State Administration of Work Safety. Training and assessment materials for main hoist driver operator qualification. 2nd ed. Xuzhou: China University of Mining and Technology Press; 2011.
3. Yu Q, Ikuta S, Shimada H, Matsui K. Application of underground continuous impervious curtain to shaft lining rupture treatment in Eastern Chinese coal mines. Mem Fac Eng Kyushu Univ. 2012;72(2):39–53.
4. Jia YD, Stace R, Williams A. Numerical modelling of shaft lining stability at deep mine. Min Technol. 2013;122(1):8–19. https://doi.org/10.1179/1743286312Y.0000000022.
5. Han JH, Zou JQ, Hu CC, Yang WH. Study on size design of shaft protection rock/coal pillars in thick soil and thin rock strata. Energies. 2019;12(13):2553. https://doi.org/10.3390/en12132553.
6. Kidybinski A, Dubinski J. Strata control in deep mines. Rotterdam: A. A. Balkema; 1990.
7. Diering DH. Ultra-deep level mining: future requirements. J S Afr Inst Min Metall. 1997;97(6):249–55.
8. He MC. Rock mechanics and hazard control in deep mining engineering in China. In: Proceedings of the 4th Asian rock mechanics symposium. Singapore: World Scientific Publishing Co. Ltd; 2006. p. 29–46.
9. Chen X, Li W, Yan X. Analysis on rock burst danger when fully-mechanized caving coal face passed fault with deep mining. Saf Sci. 2012;50(4):645–8. https://doi.org/10.1016/j.ssci.2011.08.063.
10. He MC, Xie HP, Peng SP, Jiang YD. Study on rock mechanics in deep mining engineering. Chin J Rock Mech Eng. 2005;24(16):2803–13.
11. He MC, Qian QH. Summarize of basic research on rock mechanics and engineering disaster control at great depth. In: Proceedings of the advanced seminar on prevention and control of sudden geological disasters and disaster reduction countermeasures research. Shenzhen; 2006. p. 21–45.
12. Wang M. Experiment study on characteristic of deformation and failure of roadway's surrounding rock and its controlling technique in deep mine. Dissertation, Liaoning Technical University; 2010.
13. Xie HP. Research review of the state key research development program of China: deep rock mechanics and mining theory. J China Coal Soc. 2019;44(05):1283–305. https://doi.org/10.13225/j.cnki.jccs.2019.6038.
14. Han JH, Yang QW, Yang WH. Mechanism of fracturing in shaft lining caused by mining subsidence in thin bedrock and deep loose strata. J Min Saf Eng. 2021;38(04):784–90. https://doi.org/10.13545/j.cnki.jmse.2020.0027.
15. Cheng H, Zhang LL, Yao ZS. Mechanism of shaft deflection caused by asymmetric mining in thin bedrock and deep loose strata. J China Coal Soc. 2022;47(1):102–14. https://doi.org/10.13225/j.cnki.jccs.2021.1510.
16. Zuo JP, Chen ZH, Wang HW, Liu XP, Wu ZP. Experimental investigation on fault activation pattern under deep mining. J China Coal Soc. 2009;34(3):305–9.
17. Hu QF, Cui XM, Liu WK, Ma TJ, Geng HR. Law of overburden and surface movement and deformation due to mining super thick coal seam. J Min Strata Control Eng. 2020;2(2):31–9. https://doi.org/10.13532/j.jmsce.cn10-1638/td.20191113.001.
18. Liu YX, Dai HY, Jiang YD. Model test for mining-induced movement law of rock and soil mass under thick unconsolidated layers. J Min Saf Eng. 2012;29(5):700–6.
19. Zelikson A. Geotechnical models using the hydraulic gradient similarity method. Géotechnique. 1969;19(4):495–508. https://doi.org/10.1680/geot.1969.19.4.495.
20. Ding JS, Tang QM, Long YM. Investigation of behaviour of saturated foundation soil under footing pressure by hydraulic gradient model test. J Geotech Eng. 1994;16(1):8–20.
21. Huang F, Huang WF, Li GX, Lu H. Seepage force model test on friction resistance of piles under different load conditions. Chin J Geotech Eng. 1998;20(2):3–5.
22. Yuan BX, Chen R, Yang XQ, Luo QZ, Peng T, Wang YX, Chen WW. Investigation of laterally loaded pile based on the hydraulic gradient model test. Chin J Rock Mech Eng. 2006;35(S2):4295–301. https://doi.org/10.13722/j.cnki.jrme.2016.0802.
23. Cui GX. Similarity theory and model test. Xuzhou: China University of Mining and Technology Press; 1990.
24. Liu BC, Liao GH. Basic laws of coal mine surface movement. Beijing: China Industry Press; 1965.

Publisher's Note Springer Nature remains neutral with regard to jurisdictional claims in published maps and institutional affiliations.

Discover